ACS OMEGA

http://pubs.acs.org/journal/acsodf

Article

Effective CO_2 Capture and Selective Photocatalytic Conversion into CH_3OH by Hierarchical Nanostructured GO−TiO_2−Ag_2O and GO−TiO_2−Ag_2O−Arg

Aliakbar Nosrati, Shahrzad Javanshir,* Farzaneh Feyzi, and Sara Amirnejat

Cite This: *ACS Omega* 2023, 8, 3981−3991

Read Online

ACCESS | Metrics & More | Article Recommendations | Supporting Information

ABSTRACT: The attenuation of greenhouse gases, especially CO_2, as one of the main causes of global warming and their conversion into valuable materials are among the challenges that must be met in the 21st century. For this purpose, hierarchical ternary and quaternary hybrid photocatalysts based on graphene oxide, TiO_2, Ag_2O, and arginine have been developed for combined CO_2 capture and photocatalytic reductive conversion to methanol under visible and UV light irradiation. The material's band gap energy was estimated from the diffuse reflectance spectroscopy (DRS) Tauc analysis algorithm. Structural and morphological properties of the synthesized photocatalysts were studied using various analytical techniques such as Fourier transform infrared (FTIR) spectroscopy, X-ray diffraction (XRD), scanning electron microscopy (SEM), and transmission electron microscopy (TEM). The calculated band gaps for GO−TiO_2−Ag_2O and GO−TiO_2−Ag_2O−Arg were 3.18 and 2.62 eV, respectively. This reduction in the band gap showed that GO−TiO_2−Ag_2O−Arg has a significant visible light photocatalytic ability. The investigation of CO_2 capture for the designed catalyst showed that GO−TiO_2−Ag_2O−Arg and GO−TiO_2−Ag_2O have high CO_2 absorption capacities (1250 and 1185 mmol g^{-1}, respectively, at 10 bar and 273 K under visible light irradiation). The amounts of methanol produced by GO−TiO_2−Ag_2O and GO−TiO_2−Ag_2O−Arg were 8.154 and 5.1 μmol·gcat^{1}·h^{-1} respectively. The main advantages of this study are the high efficiencies and selectivity of catalysts toward methanol formation. The reaction mechanism to understand the role of hybrid photocatalysts for CO_2 conversion is deliberated. In addition, these catalysts remain stable during the photocatalytic process and can be used repeatedly, proving to be enlightening for environmental research.

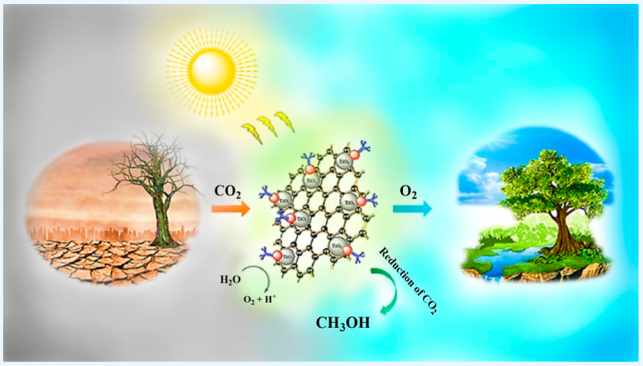

1. INTRODUCTION

In recent years, climate change has been admitted, following a quasi-scientific consensus, not only as a reality, but also as a new issue to which our societies, threatened by its consequences, must find a solution. The causal relationship between anthropogenic emission of greenhouse gases and global warming has now been established by the vast majority of experts.[1] Among the greenhouse gases, that is, H_2O, CO_2, CH_4, N_2O, and O_3, CO_2 is responsible for more than 60% of the greenhouse effect. Consequently, it is imperative to reduce CO_2 emissions and minimize the possibility of destructive global warming. CO_2 capture and its reduction into value-added products and fuels is an important emissions reduction technology to address global warming and energy needs. Due to the high stability of CO_2 and the complexity of the reactions for its transformation, the practical implementation of these methods requires the development of effective, inexpensive, stable, and selective catalysts. Different methods for the reduction and conversion of CO_2 into value-added products have been explored, including biodegradation by plants and algae and thermal, electrochemical, or photocatalytic reductions in which CO_2 is converted into value-added products.[2−5] Among these, artificial photosynthesis, which consists of reproducing and improving the processes and mechanisms at work in plants, could well be the origin of a scientific and industrial revolution (Figure 1).[6] These objectives can be achieved by the design of innovative semiconductor photocatalysts. The photocatalytic process consists of producing electron/hole (e^-/h^+) pairs, e^-/h^+ recombination, and capture of photogenerated e^-/h^+ by the adsorbed compound at the surface of the semiconductor photocatalyst, resulting in reduction and/or oxidation reactions. The rapid recombination of the e^-/h^+ pair is disadvantageous to the whole process and

Received: October 20, 2022
Accepted: January 5, 2023
Published: January 16, 2023

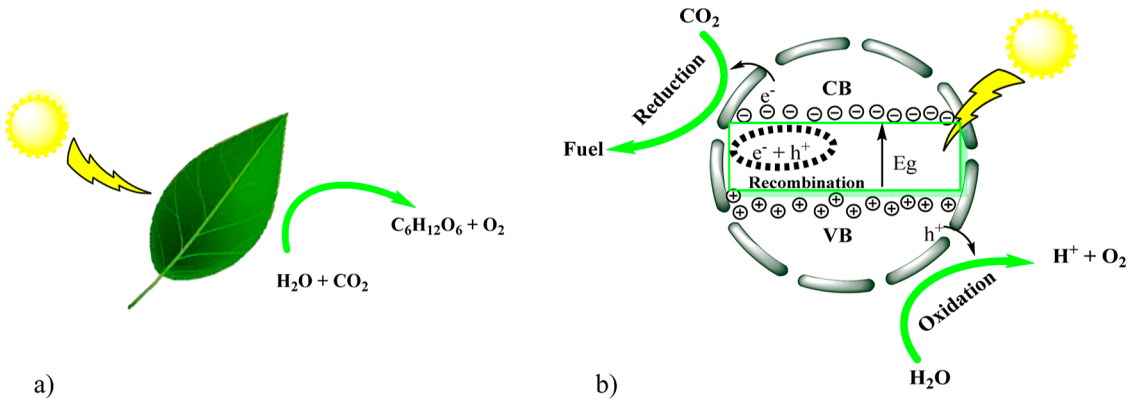

Figure 1. (a) Photosynthesis and (b) artificial photosynthesis.

limits the photocatalytic efficiency.[7−9] A number of semiconductor photocatalysts have been widely used for the reduction of CO_2 into fuels, such as TiO_2, CdS, ZnO, and In_2O_3. Among them, TiO_2 has attracted a lot of attention as a photocatalyst due to its lower cost.[10−15] Nonetheless, TiO_2 exhibits weak performance due to the fast electron/hole (e^-/h^+) pair recombination rate and large band gap energy, being active only under UV light irradiations, disadvantages that need to be overcome to become an active photocatalyst.[9,16−20] To overcome some of these limitations, different approaches can be considered such as (i) adding a sacrificial agent, (ii) depositing metallic nanoparticles, or (iii) the use of semiconductors with a narrow band gap.[21−24] Due to their higher absorption rate, lower toxicity, and higher stability, amines have been used, as a sacrificial electron donor, in the field of artificial photosynthesis by researchers from the 1970s to the present day.[25,26] The use of sacrificial amines allows the photoreduction of CO_2 to take place, when the position of the valence band (VB) of the photocatalysts is negative compared to the standard oxidation potential of H_2O, and at the same time accelerates the separation rates of the electron−hole pairs and therefore improves the photoreduction of CO_2.[26−30] Graphene oxide (GO) is another very favorable option in the photocatalytic field, which contributes to the effective degradation of CO_2. The excellent absorption and conductivity capacity of GO in combination with TiO_2 can be considered a versatile composite for photocatalysts.[15,31−34] Considering the above-mentioned facts, in our study, we developed a photocatalytic system based on titanium dioxide (TiO_2) associated with GO, using arginine as a sacrificial agent. For this purpose, hierarchical ternary and quaternary hybrid photocatalysts based on GO, TiO_2, Ag_2O, and arginine have been developed for combined CO_2 capture and photocatalytic reductive conversion to methanol under visible and UV light irradiation. The creation of a heterojunction between TiO_2 and Ag_2O allows for overcoming the limitation of the photocatalytic activity of TiO_2. Indeed, the association of these narrower gap semiconductors will not only allow an extension of the activation spectrum of composites in the visible range but also an optimal delocalization of the photo-induced charges.[33,35−37] The participation of different components in the designed photocatalyst leads to synergistic effects favorable to the photoreduction of CO_2 into methanol.

2. EXPERIMENTAL SECTION

All chemicals were provided by Merck and Sigma-Aldrich and were used without further purification. Melting points were determined using the Electrothermal 9100 apparatus. Sonication for the synthesis of the catalyst was performed using Elma at 60 Hz. The Fourier transform infrared (FTIR) spectra were obtained through a Shimadzu IR-470 spectrophotometer. The X-ray diffraction (XRD) pattern was obtained using a D8-Advance Bruker. The scanning electron microscopy (SEM) images of the photocatalyst were recorded via a TESCAN instrument. Transmission electron microscopy (TEM) images were provided using a Philips EM208S. Elemental analysis of the photocatalytic was performed by energy-dispersive X-ray spectroscopy (EDS) analysis using a TESCAN4992. Gas chromatography (GC) was performed using a Shimadzu GC 2010. Diffuse reflectance spectroscopy (DRS) was performed using a Shimadzu 2550, 220 V.

2.1. Preparation of Graphene Oxide. GO was prepared using a modified Hummer's method. In a typical procedure, 1 g of graphite powder and 1 g of sodium nitrate were dispersed in 23 mL of sulfuric acid (98%) in a vessel, and the mixture was stirred at 66 °C for 1 h. The reaction vessel was then immersed in an ultrasonic bath for 30 min to thoroughly disperse the particles in the reaction medium. The temperature of the ultrasonic bath was cooled down to 10 °C by adding ice. Next, powdered potassium permanganate ($KMnO_4$, 3 g) was slowly added to the reaction vessel for over 1 h under magnetic stirring. During the addition of $KMnO_4$, the reaction vessel was placed in an ice bath to keep the temperature below 10 °C. Subsequently, the ice bath was removed, the temperature was increased to 35 °C, and the reaction mixture was stirred for 30 min, after which 50 mL of water was slowly added. The reaction medium was then heated at 98 °C for 30 min, leading to a brown suspension. The brown suspension was diluted with 700 mL of distilled water and then treated with 12 mL of H_2O_2 (30%). After the addition of H_2O_2, a bright yellow color was observed, which determined that the reaction was completed and graphite was converted into graphite oxide. The reaction mixture was centrifuged, washed with deionized water and HCl (5%) repetitively, and dried at 60 °C.[38,39]

2.2. Preparation of TiO_2−Ag_2O. Titanium oxide (TiO_2, 0.24 g, 3 mmol) was dispersed in an aqueous solution of silver nitrate ($AgNO_3$, 22 mL, 0.023 M), and the suspension was stirred for 1 h. The suspension was then exposed to UV light (UV lamp 254 nm, the intensity of 5.4 mW/cm^2) under stirring for 15 min. The pH of the mixture was adjusted to 9 by dropwise addition of 0.5 M NaOH. The TiO_2−Ag_2O precipitate was washed with deionized water until neutralization and dried in an oven at 80 °C.[40]

https://doi.org/10.1021/acsomega.2c06753
ACS Omega 2023, 8, 3981−3991

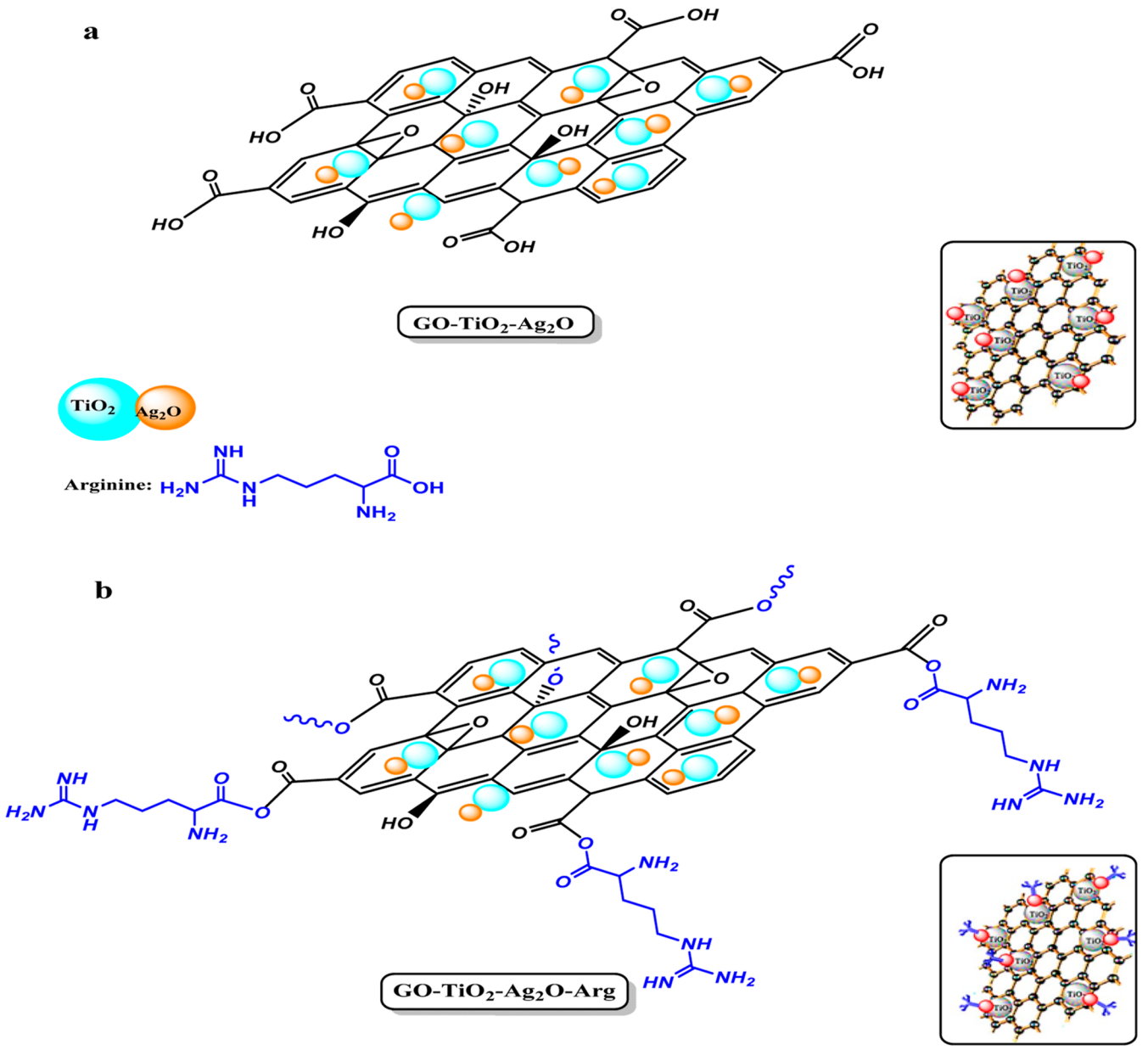

Figure 2. (a) General structure GO−TiO_2−Ag_2O and (b) general structure GO−TiO_2−Ag_2O−Arg.

2.3. Preparation of GO−TiO_2−Ag_2O. TiO_2−Ag_2O (1 mg) was fully dispersed in MeOH (35 mL) by probe sonication (90 watts) for 90 min. Then, 0.3 mg of GO was added, and probe sonication was applied for 10 min. The resulting dispersion was stirred at room temperature by magnetic stirring for 24 h and then dried in the oven at 60 °C (Figure 2a).

2.4. Preparation of GO−TiO_2−Ag_2O−Arg. 0.2 g of GO−TiO_2−Ag_2O was dispersed in 10 mL of distilled water using probe sonication for 90 min (90 watts). Then, 0.4 g of L-arginine (Arg) was added and sonicated for 30 min. The reaction medium was then refluxed under stirring for 5 h. The obtained GO−TiO_2−Ag_2O−Arg was kept in the oven at 60 °C to dry (Figure 2b).

2.5. Photocatalytic Procedure for the CO_2 Capture and Conversion to Methanol. The apparatus used for the photocatalytic absorption/reaction of CO_2 is schematically shown in Figure 3. The reactions were carried out under UV and visible light radiation. The UV light photoreaction was carried out in a Pyrex glass photoreactor with a volume capacity of 100 mL, equipped with a water circulation jacket (model LAUDA ALPHA RA8 with a temperature accuracy of ±0.1 K) and a magnetic stirrer. Depending on the type and purpose of the test, the visible or ultraviolet light source was used. The light source was located at a constant distance from the reactor. The reactor was evacuated before each experiment was run using a vacuum pump. CO_2 was provided from a storage tank and a stainless-steel gas container with an approximate volume of 445.106 cm^3, which was installed between the storage tank and the photoreactor.

Valves were used to control the CO_2 flow from the storage and gas container to the photoreactor. The temperature of the gas container was measured using a Chromel-Alumel Type K with an accuracy of ±0.1 K. The pressure inside the photoreactor and the gas container was measured using two pressure sensors (model BD Sensor with an accuracy of ±1

https://doi.org/10.1021/acsomega.2c06753
ACS Omega 2023, 8, 3981−3991

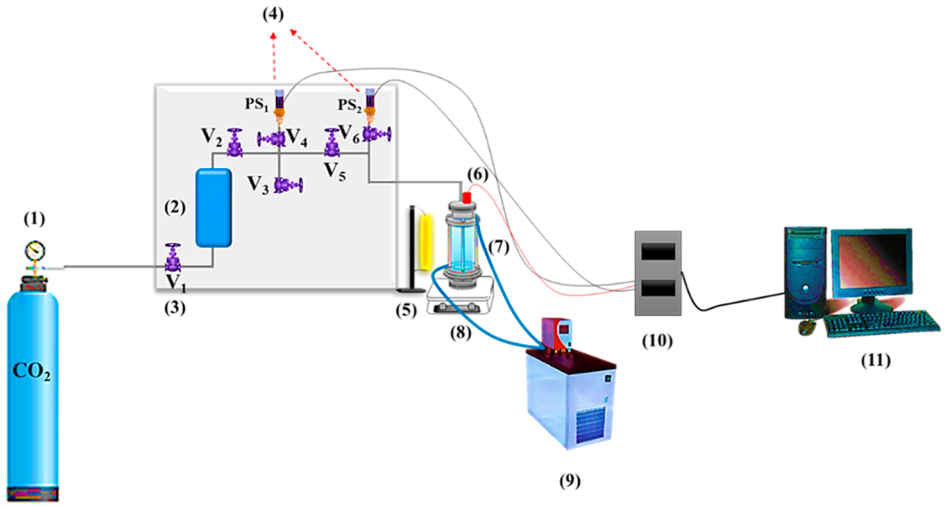

Figure 3. Experimental setup for measuring CO_2 absorption: (1) CO_2 cylinder, (2) gas container, (3) (V1−V6) valves, (4) (PS1 and PS2) pressure sensors, (5) visible or UV light source, (6) thermometer, (7) reaction reactor, (8) magnetic stirre,r (9) circulating water bath, (10) monitor and interface, and (11) computer.

kPa). Temperature and pressure transmitters were connected to a personal computer in which the temperature and pressure data were recorded. By adjusting the valves, CO_2 gas was introduced into the reactor.[41,42] Equilibrium was reached when the pressure and the temperature inside the photoreactor reached a constant value. The initial and final pressures of CO_2 in the photoreactor were used to calculate the amount of CO_2 absorbed. For details of the procedure and calculations, we refer the readers to refs 41 and 42 and the next subsection.

2.5.1. Photocatalytic Capture of CO_2. The photocatalyst (0.4 g) was placed in the Pyrex glass reactor containing 80 mL of dimethylformamide (DMF). CO_2 was introduced and allowed to flow in contact with the catalyst to achieve a sorption equilibrium. The average optimal time for each test under UV and visible light was 4 h. The amount of absorbed CO_2 (α), was calculated using eq 1[43]

$$\alpha = \frac{n^{l}_{CO_2}}{n_{DMF}} \tag{1}$$

where n_{DMF} denotes the moles of DMF and $n^{l}_{CO_2}$ represents the moles of absorbed CO_2, which was calculated from eq 2, where n_{CO_2} represents the moles of injected CO_2 into the photoreactor and $n^{g}_{CO_2}$ represents the moles of unabsorbed CO_2 in the gas phase, calculated using eqs 3 and 4

$$n^{l}_{CO_2} = n_{CO_2} - n^{g}_{CO_2} \tag{2}$$

$$n_{CO_2} = \frac{V_{gc}}{R}\left(\frac{P_1}{Z_1T_1} + \frac{P_2}{Z_2T_2}\right) \tag{3}$$

where R is the universal gas constant and Z is the gas compressibility factor calculated by the Peng−Robinson equation of state.[44] V_{gc}, P, and T are the volume, pressure, and temperature of the gas inside the reactor, respectively. Subscripts 1 and 2 refer to before and after CO_2 injection, respectively.

$$n^{g}_{CO_2} = \frac{(V - V_s)(P_{eq})}{Z_{CO_2} - RT} \tag{4}$$

In eq 4, V and V_s are the volume of the reactor and the volume of the solvent, respectively. P_{eq}, designates the pressure of the nonabsorbed CO_2, that is, the difference between the pressure before and after the absorption of CO_2. The data and the corresponding diagrams are presented in Section 3.2.

2.5.2. Photoreduction of CO_2 to CH_3OH under UV/Visible Light. For the conversion of CO_2 to methanol under ultraviolet and visible light, 0.1 g of the catalyst was transferred to the reactor containing DMF (18 mL) and a magnetic stirrer. To increase the solubility of CO_2, an aqueous NaOH solution (1 mL, 0.1 M) was added to the reaction mixture. The photoreactor was then connected to the CO_2 pressure regulator, and a specific volume of CO_2 was injected into the reactor. During the photocatalytic production of methanol, the maximum reaction temperature reaches 40 °C, under visible or ultraviolet light, which is in the appropriate temperature range according to previous reports.[45−47] Once the reaction was complete, samples were removed from the photoreactor using a pipette, and after being centrifuged, they were subjected to GC analysis to determine the amount of methanol produced.

3. RESULTS AND DISCUSSION

3.1. Characterization of the Catalysts. Figure 4 illustrates the FTIR spectra of GO, GO−TiO_2−Ag_2O, and GO−TiO_2−Ag_2O−Arg. The FTIR spectrum of GO shows an absorption band at ∼3400 cm^{-1} and other peaks at 1736 and 1620 cm^{-1}, corresponding to OH, C═O, and C−O stretching. The absorption band observed at 550−750 cm^{-1}, in both GO−TiO_2−Ag_2O and GO−TiO_2−Ag_2O−Arg, is due to the metal−oxygen vibrations. The peaks at ∼1640 and 3400 cm^{-1} correspond to the deforming and stretching vibration of OH, respectively. The existence of a very broad absorption band in the spectrum of GO−TiO_2−Ag_2O−Arg from 2600 to 3700 cm^{-1} is due to the O−H, N−H, and saturated C−H stretching overlaps. The broad absorption band at 1550 to 1750 cm^{-1} is due to the C═O and C−O stretching vibrations, as well as N−H bending vibrations regarding Arg.

The morphology, crystal structure, and composition of the prepared catalysts were studied using SEM, XRD, and EDS analyses. SEM images of TiO_2−Ag_2O, GO−TiO_2−Ag_2O, and GO−TiO_2−Ag_2O−Arg are shown in Figure 5a−c. Figure 5a

https://doi.org/10.1021/acsomega.2c06753
ACS Omega 2023, 8, 3981−3991

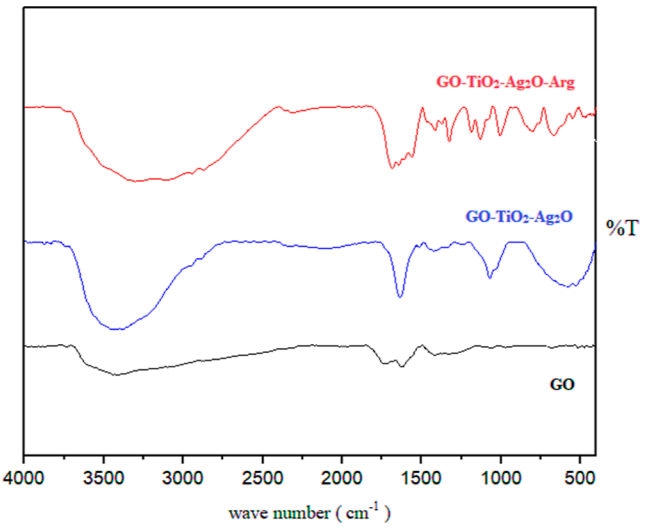

Figure 4. FTIR spectra of GO, GO−TiO_2−Ag_2O, and GO−TiO_2−Ag_2O−Arg.

reveals that the TiO_2−Ag_2O surface has a porous structure and Ag_2O nanoparticles are evenly loaded on TiO_2.

The SEM image of GO−TiO_2−Ag_2O (Figure 5b) reveals the almost uniform deposition of TiO_2/AgO_2 particles on the surface of GO sheets. The change in the morphology observed in the SEM image of GO−TiO_2−Ag_2O−Arg (Figure 5c) confirms the addition of the amino acid arginine.

Figure 6a illustrates the XRD model of GO−TiO_2−Ag_2O. As can be seen, all the peaks can be attributed to TiO_2, Ag_2O, and GO according to the standard models JCPDS 00-001-1292, JCPDS 43-0997, and JCPDS 75-2078 respectively. The two peaks at 2θ values of 25.4 and 26.7 in the XRD pattern of GO−TiO_2−Ag_2O, matching to anatase (101) and rutile (110) phases, respectively, prove the biphasic nature of TiO_2. L-arginine has an amorphous structure that causes a large bump distributed in a wide 2θ range in the XRD pattern of the sample (Figure 6b).

The EDS analysis was carried out to determine the surface elemental composition of GO−TiO_2−Ag_2O, giving a general mapping of the sample. As depicted in Figure 7 the presence of C, O, Ti, and Ag can be easily identified; C and O atoms can be attributed to GO and metal oxide.

The shape and size distributions of GO−TiO_2−Ag_2O were evaluated by TEM analysis. TEM images with different magnifications (50, 100, 200, and 300) are shown in Figure 8. The presence of black dots on the GO sheets is apparent. Proper distribution of metal oxides is observed throughout the GO layers, which increases the interactive role of the constituent components in the catalyst structure. This distribution of metal oxide nanoparticles on GO sheets can generate local active sites and facilitate the photocatalytic reaction. As shown on the 100 nm scale, the Ag_2O particles are

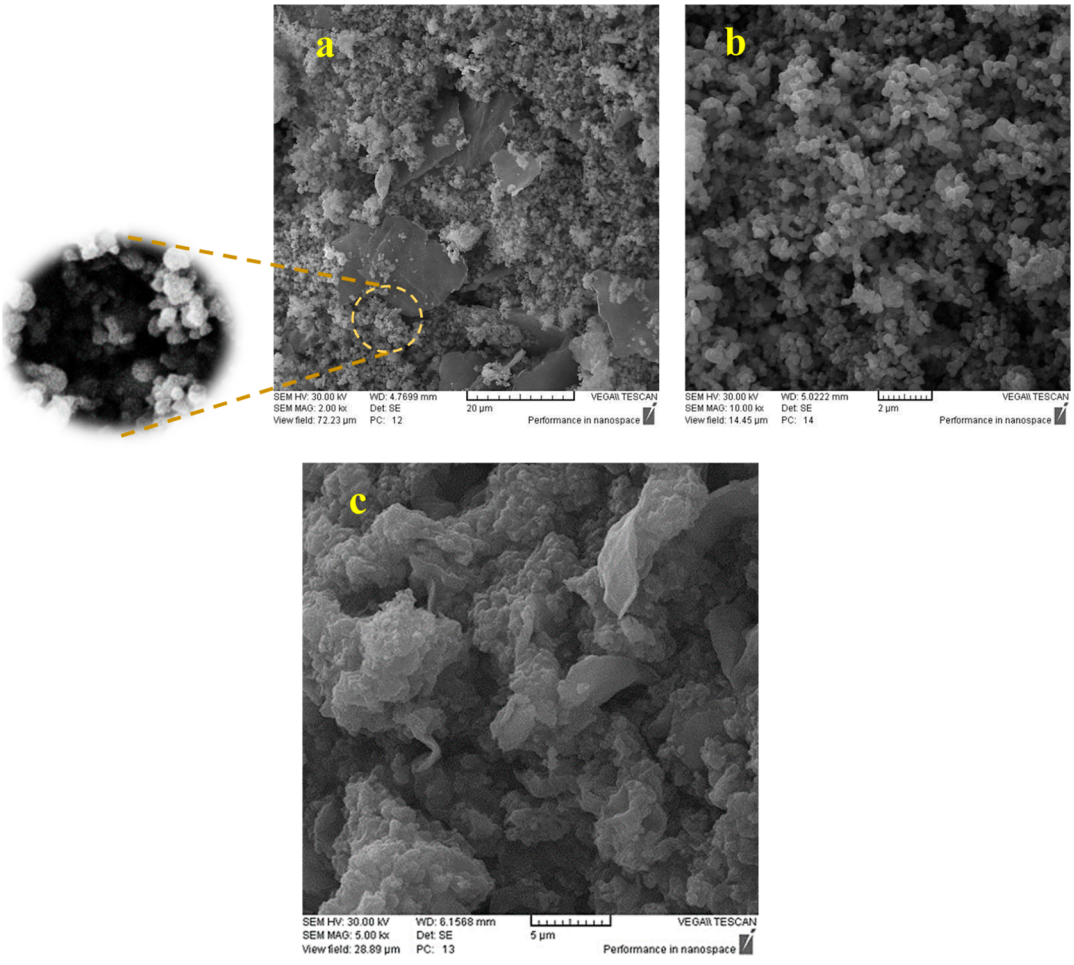

Figure 5. SEM images of (a) TiO_2−Ag_2O; (b) GO−TiO_2−Ag_2O; and (c) GO−TiO_2−Ag_2O−Arg.

https://doi.org/10.1021/acsomega.2c06753
ACS Omega 2023, 8, 3981−3991

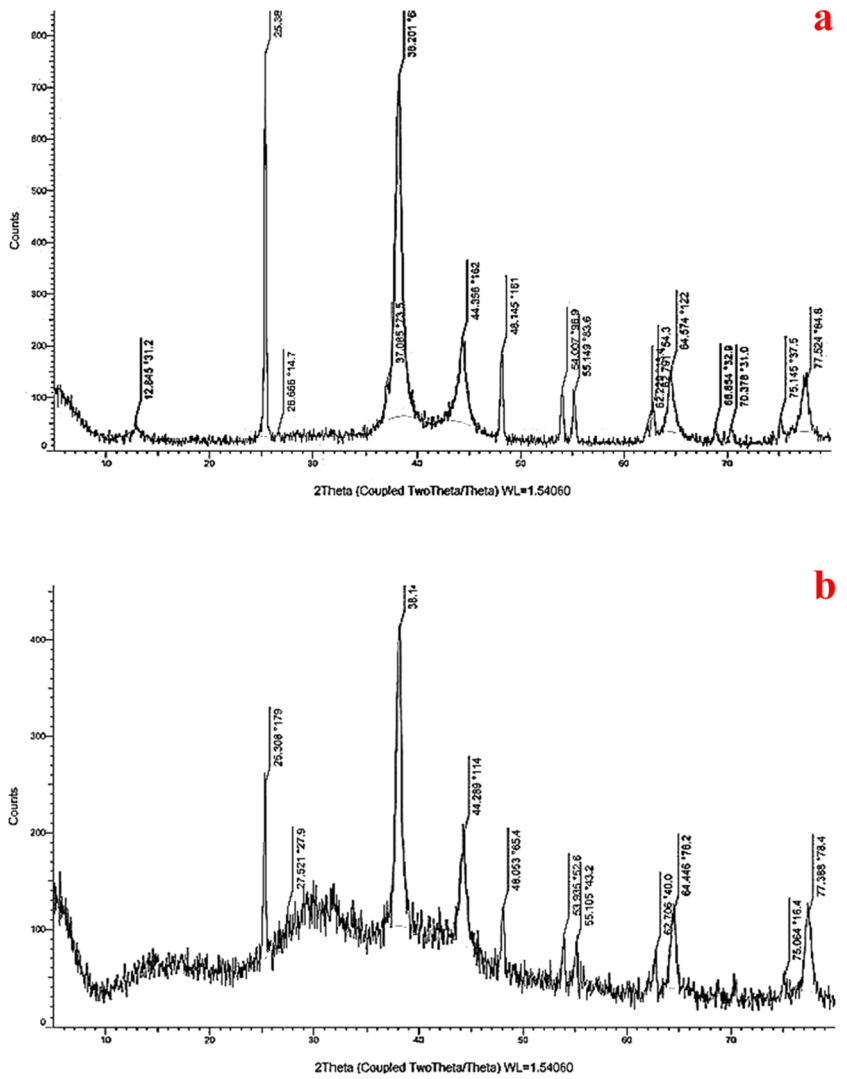

Figure 6. XRD patterns of (a) GO−TiO_2−Ag_2O and (b) GO−TiO_2−Ag_2O−Arg.

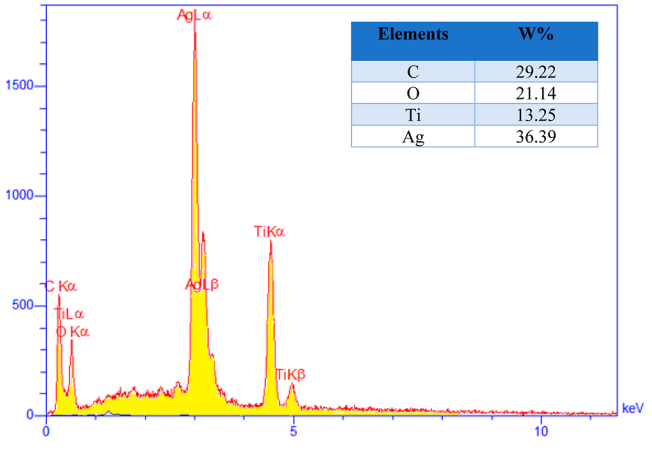

Figure 7. EDS analysis of GO−TiO_2−Ag_2O.

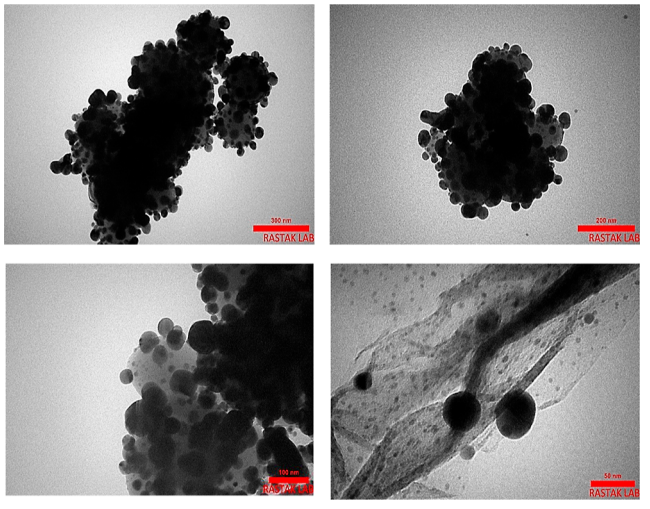

Figure 8. TEM images of GO−TiO_2−Ag_2O with different magnifications.

located next to and on the TiO_2 particles; also, as shown on the 50 nm scale, TiO_2 and Ag_2O are located on the GO surface, which not only confirms the correct placement of the metal oxides together but also results in better electronic transmission.

3.2. Diffuse Reflectance Spectroscopy. The optical properties of GO−TiO_2−Ag_2O and GO−TiO_2−Ag_2O−Arg were investigated by UV/vis diffuse reflectance spectroscopy

https://doi.org/10.1021/acsomega.2c06753
ACS Omega 2023, 8, 3981−3991

[Figure S1a (see the Supporting information)]. Tauc plots were employed to estimate the band gap of the semiconductor samples. The band gaps of GO−TiO_2−Ag_2O and GO−TiO_2−Ag_2O−Arg were 3.18 and 2.62 eV, respectively, as exhibited in Figure S1b,c. Consequently, the GO−TiO_2−Ag_2O photocatalyst is more active in the UV region, while the activity of GO−TiO_2−Ag_2O−Arg is extended into the visible spectrum due to its lower band gap energy. The addition of arginine (Arg) alongside the combination of rutile and anatase phases improved the degree of absorption of visible light and thus enhanced the photocatalytic performance of the catalyst.

3.3. Photoluminescence Spectroscopy. The photoluminescence of the GO−TiO_2−Ag_2O catalyst illustrates that the emission position is from 380 to 450 nm [Figure S2a (see the Supporting information)]. In comparison, the emission for the GO−TiO_2−Ag_2O−Arg catalyst appears at a position in wavelength range from 350 nm to about 500 nm [Figure S2b (see the Supporting information)]. It should be noted that the GO−TiO_2−Ag_2O−Arg catalyst has a larger PL absorption surface than the GO−TiO_2−Ag_2O catalyst, which results in better photocatalytic activity in the visible region (Figure S2b).

3.4. Investigation of the Amount of CO_2 Absorption by Catalysts under Different Conditions. The absorbing capacity is defined as the maximum molar amount of CO_2 absorbed per mole of the photocatalytic activity for capture and reduction of CO_2 to methanol under UV and visible light irradiation using the as-prepared GO−TiO_2−Ag_2O and GO−TiO_2−Ag_2O−Arg catalysts. The amount of CO_2 capture was examined in the presence of GO−TiO_2−Ag_2O and GO−TiO_2−Ag_2O−Arg catalysts under UV and visible light irradiation, at different temperatures using different solvents. The results are presented in the form of an absorption pressure diagram. The vertical axis represents the equilibrium pressure (the pressure of CO_2 not being absorbed into the reactor), and the horizontal axis represents the rate of absorption of CO_2 per mole of the solvent (α). A higher value of α indicates better and greater absorption of gas by the catalyst. For each experiment, seven injections were carried out. The rate of gas absorption varies depending on the solvent, catalyst, temperature, and light.

Figure S3 shows the CO_2 absorption measured at 40 °C under ultraviolet light, using 0.04 g of the photocatalyst. The results revealed that the absorption of CO_2 in the presence of GO−TiO_2−Ag_2O is higher than in the presence of GO−TiO_2−Ag_2O−Arg due to the proportionality of the energy gap of GO−TiO_2−Ag_2O and ultraviolet light. The CO_2 absorption under visible light is presented in Figure S4. The absorption performance of GO−TiO_2−Ag_2O−Arg was better than that of the pure solvent as well as GO−TiO_2−Ag_2O. In another experiment, the effect of light on the catalysts and their absorption at ambient temperature was investigated. The amount of the catalyst used is 0.04 g (Figure S5). As can be seen from these graphs, the rate of catalyst absorption in the light is much higher than that in the dark, which is another confirmation of the sensitivity of the light to the synthesized catalysts and their better performance in light than in darkness.

In another study to determine whether arginine amino acids are capable of absorption or all of these absorption processes proceed by an optical mechanism, a comparison was made between CO_2 absorption without arginine by the GO−TiO_2−Ag_2O−Arg catalyst. The amounts of each of the substances used in this experiment were 0.04 g. As can be seen, the absorption rate of an arginine-functionalized catalyst is much higher than that of arginine. As can be seen, the absorption rate of an arginine-functionalized catalyst is much higher than that of arginine (Figure S6).

To evaluate the recyclability of the photocatalyst, they were reused at room temperature and under visible light for CO_2 capture, and the results showed that the performance of the catalyst did not drop significantly (Figures S7 and S8).

As shown in Figure S8, the CO_2 absorption rate for the reused catalyst has not changed significantly compared to that of the fresh catalyst; therefore, the catalyst can be reused several times with significant activity.

The obtained results revealed that GO−TiO_2−Ag_2O−Arg shows enhanced activity under visible light compared to GO−TiO_2−Ag_2O, which is in agreement with the results obtained for the band gaps. The comparison of the performance of the two catalysts in the presence of light and in the dark also revealed that the process of CO_2 absorption by the catalysts is considerably improved by light.

According to Table 1, the highest absorption of CO_2 is observed for GO−TiO_2−Ag_2O−Arg at ambient temperature under visible light, while GO−TiO_2−Ag_2O exhibits a higher absorption of CO_2 at ambient temperature under UV light. However, overall, the GO−TiO_2−Ag_2O−Arg catalyst showed higher absorption. The chemical reaction between CO_2 and arginine, which has been grafted on the surface of the photocatalyst, would limit the presence of CO_2 in the molecular form in the solvent and therefore reduce the partial pressure of CO_2 at equilibrium and would increase the concentration gradient of CO_2 at the gas−liquid interface and therefore increase the absorption flux. The absorption performance also depends on the contact temperature and was improved at room temperature, leading to better absorption of CO_2 in the liquid phase.

Table 1. Comparison of CO_2 Absorption Capacity of the Catalysts under Different Conditions at 10 bar

entry	catalyst	temp (°C)	light	CO_2 absorption (mmol/g)
1	GO−TiO_2−Ag_2O−Arg	r.t.	UV	1237.815
		40	UV	690.27
		r.t.	vis	1255.461
		40	vis	786.544
		r.t.	dark	988.296
2	GO−TiO_2−Ag_2O	r.t.	UV	1209.27
		40	UV	988.695
		r.t.	vis	1183.32
		40	vis	621.502
		r.t.	dark	910.845

3.5. Photoreduction of CO_2 to CH_3OH. Following a series of experiments on CO_2 absorption and conversion, CO_2 was converted to methanol at this step of the reaction under visible light for the catalyst of GO−TiO_2−Ag_2O−Arg and ultraviolet light for the catalyst of GO−TiO_2−Ag_2O at 40 °C, performed separately. Finally, the amount of the product produced by each of the catalysts was measured by GC. The GC results from the two catalysts GO−TiO_2−Ag_2O−Arg and GO−TiO_2−Ag_2O are shown (Figures S9 and S10). The standard pure solvent courier is also shown (Figure S11).

As can be seen, in about 3:30 min, a courier related to methanol is observed, which is completely consistent with the courier from the standard methanol sample, and they appear in

https://doi.org/10.1021/acsomega.2c06753
ACS Omega 2023, 8, 3981−3991

an instant. The next long peak that has been removed from the frame is related to the DMF solvent, which is quite natural due to the high concentration of the solvent (Figures S9 and S10).

Also, in order to ensure that arginine amino acid without a substrate could not produce methanol, a test was performed with 0.1 g of arginine and the same test conditions were applied with other catalysts, which showed that no methanol was produced in this experiment, which shows that arginine amino acid does not have the ability to synthesize methanol under the same conditions (Figure S12).

As can be seen from the data in Table 2, the amount of the surface area under the peak for the non-functionalized catalyst was higher than that for the functionalized catalyst with arginine. The amount of methanol produced in the presence of GO−TiO_2−Ag_2O under ultraviolet light was 32.616, and it was 20.385 μmol/g_{Cat} in the presence of GO−TiO_2−Ag_2O−Arg under visible light. A comparison of photocatalyst activity was made with that of previously reported catalysts for the formation of methanol, and the results are tabulated in Table 3. As can be seen, the small amount of methanol produced by most photocatalysts under visible light is a significant drawback, limiting their practical application in the reduction of CO_2 to methanol. Some of the reported photocatalysts (entries 2 and 3) showed only a good conversion rate in a UV light environment.

Table 2. Surface Area of the Methanol Peak Produced by the Catalysts

catalyst	the area below the methanol peak
GO−TiO_2−Ag_2O(0.1 g)	2,601,501.7
GO−TiO_2−Ag_2O−Arg(0.1 g)	1,725,104.5
arginine (0.1 g)	0

3.6. Probable Photocatalytic Mechanism. The VB and conduction band (CB) energy levels of the two semiconductors are ideally staggered, leading to a type II heterojunction. This results in a new chemical potential between the semiconductors. This phenomenon considerably increases the spatial separation of the charges on either side of the heterojunction, thus limiting the recombination of the charges and increasing the lifetime of the charge carriers. In addition, the oxidation and reduction reactions take place on two different semiconductors. The photoreactions that occurred during the photoreduction of CO_2 at the surface of GO−TiO_2−Ag_2O−Arg are presented in eqs 5−7.

$$GO - TiO_2 - Ag_2O - Arg + h\nu \rightarrow h^+ + e^- \quad (5)$$

$$H_2O + h^+ \rightarrow 1/2\ O_2 + 2H^+ \quad (6)$$

$$CO_2 + 6H^+ + 6e^- \rightarrow CH_3OH + H_2O \quad (7)$$

The CO_2 absorbed by L-arginine on the surface of the photocatalyst is reduced to CH_3OH in a multi-step process involving (i) photogeneration of electrons−hole pairs by light absorption, (ii) electron excitation, (iii) transfer to the catalyst surface, and ultimately (iv) water oxidation by the holes (Figure 9).[8,56−59]

4. CONCLUSIONS

Anthropogenic CO_2, and more particularly that emitted by the combustion of fossil resources, is at the origin of global warming. Therefore, there has been more interest in the capture and valorization of greenhouse CO_2 into value-added products. However, the development of visible light photocatalysts for CO_2 reduction into value-added products is a challenge, and heterogeneous catalysts play a key role in achieving the goals. In this article, we report a photocatalytic process for combined CO_2 capture and selective photocatalytic conversion to methanol under visible and UV light irradiation, using the newly designed hierarchical ternary and quaternary hybrid photocatalysts based on TiO_2−GO−Ag_2O and arginine as a sacrificial agent. The designed catalysts, GO−TiO_2−Ag_2O−Arg and GO−TiO_2−Ag_2O, besides promising CO_2 capture, have enhanced performance for selective photoreduction of CO_2 to methanol at 40 °C, under visible (32.616 μmol/g^{-1}) and UV (20.385 μmol·g^{-1}) light irradiation, highlighting their potential use as a novel and eco-friendly photocatalyst. These fairly remarkable performances under visible light can come from different effects: (1) the presence of a small proportion of the rutile phase of TiO_2 in composites, which makes it possible to absorb wavelengths up to 420 nm, (2) the presence of GO, authorizing the absorption of a significant part of the visible spectrum and consequently the possibility of oxidizing H_2O directly on GO, (3) the formation of the TiO_2−GO heterojunction, resulting in better charge separation and possible photosensitization of TiO_2, (4) the

Table 3. Comparison of the Activity of the Catalyst in the Synthesis of CH_3OH with That of Some of the Other Catalysts Reported in the Literature

entry	catalyst (g)	react. cond. light/time (h)	product (μmol/g catalyst)	ref.
1	V−TiO_2 (0.2)	Vis/4	CH_3OH (4.6)	48
	Cr−TiO_2 (0.2)		CH_3OH (2.94)	
	Co−TiO_2 (0.2)		CH_3OH (6.53)	
2	Ag−TiO_2 (0.1)	UV−Vis/8 and 6	CH_3OH (29)	49
			CH_3OH (15)	
3	N-doped TiO_2 (0.6)	UV−Vis/2	CH_3OH (20)	50
4	N−TiO_2 (0.1)	Vis/2	CH_3OH (0.2)	51
5	$FeTiO_3$/TiO_2 (0.05)	UV−Vis/3	CH_3OH (1.386−1.296)	52
6	Cu/Fe−TiO_2−SiO_2		CH_3OH (4.12)	53
7	Ti-sillica film		CH_4/CH_3OH (11)	54
8	g-C_3N_4 (0.1)	UV−Vis/1	CH_3OH (0.26)	55
	amine-functionalizedg-C_3N_4 (0.1)	UV−Vis/1	CH_3OH (0.28)	
9	GO−TiO_2−Ag_2O (0.1)	UV/4	CH_3OH (32.616)	this work
10	GO−TiO_2−Ag_2O−Arg (0.1)	Vis/4	CH_3OH (20.385)	this work

https://doi.org/10.1021/acsomega.2c06753
ACS Omega 2023, 8, 3981−3991

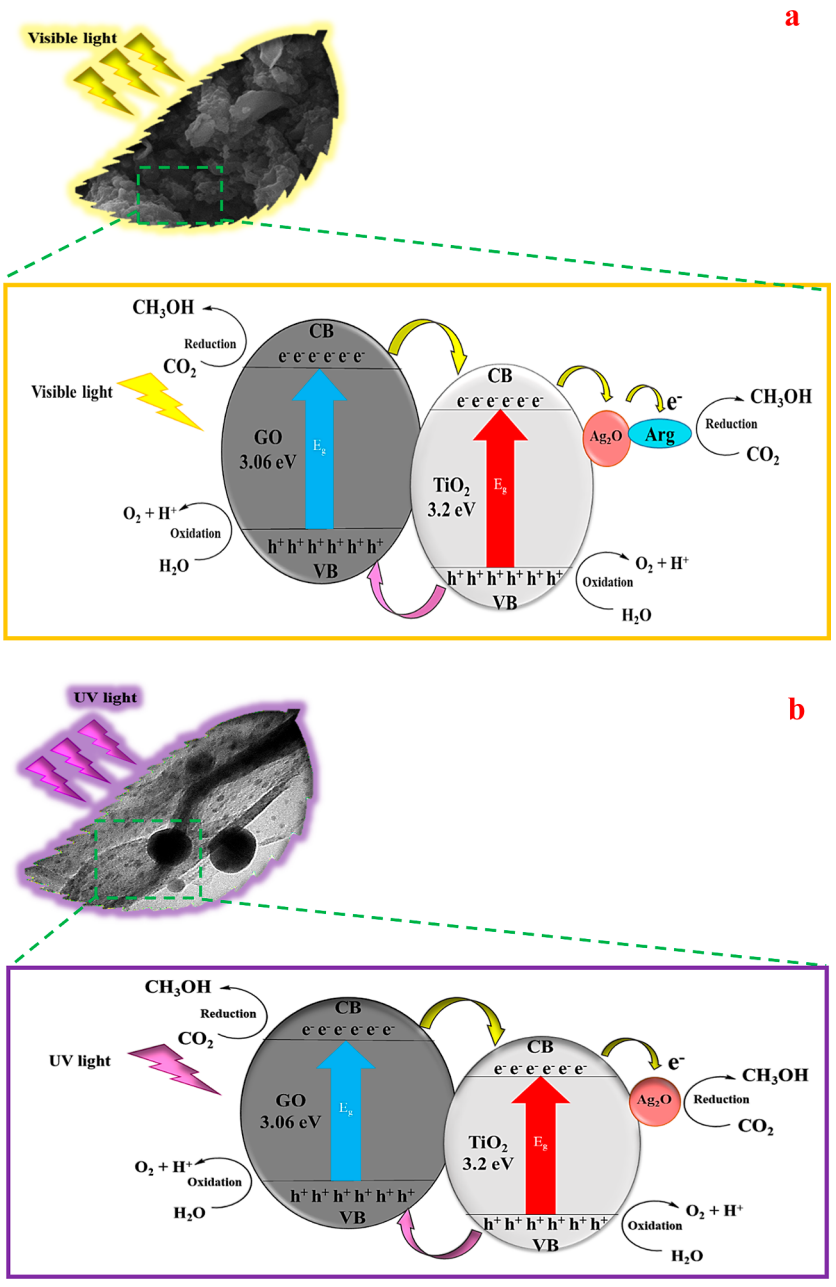

Figure 9. Schematic representation of the reaction mechanism proposed for the photoreduction of CO_2 to CH_3OH over (a) GO−TiO_2−Ag_2O−Arg composite under visible light and (b) GO−TiO_2−Ag_2O composite under UV light.

deposition of Ag_2O NPs on GO, which can induce surface plasmon resonance (SPRs) and therefore increase the number of "visible" photons absorbed by GO, and (5) the use of arginine as an effective promoter to enhance the absorption rate of CO_2. The prepared catalysts were found to be more active than the other similar catalysts previously reported.

■ ASSOCIATED CONTENT

Supporting Information

The Supporting Information is available free of charge at https://pubs.acs.org/doi/10.1021/acsomega.2c06753.

UV−vis (DRS mode) spectra of the samples, photoluminescence spectra, CO_2 absorption curves under visible and UV−vis light, and GC analysis data (PDF)

■ AUTHOR INFORMATION

Corresponding Author

Shahrzad Javanshir − *Heterocyclic Chemistry Research Laboratory, Department of Chemistry, Iran University of Science and Technology, Tehran 16846-13114, Iran;* orcid.org/0000-0002-3161-0456; Email: shjavan@iust.ac.ir

Authors

Aliakbar Nosrati − *Heterocyclic Chemistry Research Laboratory, Department of Chemistry, Iran University of Science and Technology, Tehran 16846-13114, Iran*

Farzaneh Feyzi − *Thermodynamics Research Laboratory, School of Chemical Engineering, Iran University of Science and Technology, Tehran 1684613114, Iran;* orcid.org/0000-0001-8865-7274

https://doi.org/10.1021/acsomega.2c06753
ACS Omega 2023, 8, 3981−3991

Sara Amirnejat − *Heterocyclic Chemistry Research Laboratory, Department of Chemistry, Iran University of Science and Technology, Tehran 16846-13114, Iran*

Complete contact information is available at: https://pubs.acs.org/10.1021/acsomega.2c06753

Notes

The authors declare no competing financial interest.

■ ACKNOWLEDGMENTS

The authors wish to express their gratitude for the partial financial support provided by the Research Council of Iran University of Science and Technology (IUST), Tehran, Iran.

■ REFERENCES

(1) Carapellucci, R.; Milazzo, A. Membrane systems for CO2 capture and their integration with gas turbine plants. *Proc. Inst. Mech. Eng., Part A* **2003**, *217*, 505−517.
(2) Rubin, E.; De Coninck, H.IPCC special report on carbon dioxide capture and storage. *TNO (2004): Cost Curves for CO2 Storage*; Cambridge University Press: UK, 2005; p 14. Part 2.
(3) Windle, C. D.; Perutz, R. N. Advances in molecular photocatalytic and electrocatalytic CO2 reduction. *Coord. Chem. Rev.* **2012**, *256*, 2562−2570.
(4) Sargeant, E.; Kolodziej, A.; Le Duff, C. S.; Rodriguez, P. Electrochemical conversion of CO2 and CH4 at subzero temperatures. *ACS Catal.* **2020**, *10*, 7464.
(5) Bhosale, M. G.; Sutar, R. S.; Londhe, S. S.; Patil, M. K. Sol−gel method synthesized Ce-doped TiO2 visible light photocatalyst for degradation of organic pollutants. *Appl. Organomet. Chem.* **2022**, *36*, No. e6586.
(6) Yu, S.; Jain, P. K. Plasmonic photosynthesis of C1−C3 hydrocarbons from carbon dioxide assisted by an ionic liquid. *Nat. Commun.* **2019**, *10*, 2022.
(7) Ganesh, I. Solar fuels vis-à-vis electricity generation from sunlight: The current state-of-the-art (a review). *Renew. Sustain. Energy Rev.* **2015**, *44*, 904−932.
(8) Zhao, J.; Wang, Y.; Wang, Y.; Xu, Y. Mutual influence of cupric cations and several anions in anatase and rutile TiO2 photocatalysis. *Photochem. Photobiol. Sci.* **2021**, *20*, 1099.
(9) Kamal, K. M.; Narayan, R.; Chandran, N.; Popović, S.; Nazrulla, M. A.; Kovač, J.; Vrtovec, N.; Bele, M.; Hodnik, N.; Kržmanc, M. M.; Likozar, B. Synergistic Enhancement of Photocatalytic CO2 Reduction by Plasmonic Au Nanoparticles on TiO2 Decorated N-graphene Heterostructure Catalyst for High Selectivity Methane Production. *Appl. Catal., B* **2022**, *307*, 121181.
(10) Inoue, T.; Fujishima, A.; Konishi, S.; Honda, K. Photoelectrocatalytic reduction of carbon dioxide in aqueous suspensions of semiconductor powders. *Nature* **1979**, *277*, 637−638.
(11) Roy, S. C.; Varghese, O. K.; Paulose, M.; Grimes, C. A. Toward solar fuels: photocatalytic conversion of carbon dioxide to hydrocarbons. *ACS Nano* **2010**, *4*, 1259−1278.
(12) Indrakanti, V. P.; Kubicki, J. D.; Schobert, H. H. Photoinduced activation of CO2 on Ti-based heterogeneous catalysts: Current state, chemical physics-based insights and outlook. *Energy Environ. Sci.* **2009**, *2*, 745−758.
(13) Takeda, H.; Koike, K.; Inoue, H.; Ishitani, O. Development of an Efficient Photocatalytic System for CO2 Reduction Using Rhenium(I) Complexes Based on Mechanistic Studies. *JACS* **2008**, *130*, 2023−2031.
(14) Cao, L.; Sahu, S.; Anilkumar, P.; Bunker, C. E.; Xu, J.; Fernando, K. S.; Wang, P.; Guliants, E. A.; Tackett, K. N.; Sun, Y.-P. Carbon nanoparticles as visible-light photocatalysts for efficient CO2 conversion and beyond. *JACS* **2011**, *133*, 4754−4757.
(15) Darvishnejad, M. H.; Reisi-Vanani, A. Synergetic effects of metals in graphyne 2D carbon structure for high promotion of CO2 capturing. *Chem. Eng. J.* **2021**, *406*, 126749.
(16) Neatu, S.; Maciá-Agulló, J. A.; Garcia, H. Solar light photocatalytic CO2 reduction: general considerations and selected bench-mark photocatalysts. *Int. J. Mol. Sci.* **2014**, *15*, 5246−5262.
(17) Liu, E.; Kang, L.; Wu, F.; Sun, T.; Hu, X.; Yang, Y.; Liu, H.; Fan, J. Photocatalytic reduction of CO 2 into methanol over Ag/TiO2 nanocomposites enhanced by surface plasmon resonance. *Plasmonics* **2014**, *9*, 61−70.
(18) Matijević, M.; Žakula, J.; Korićanac, L.; Radoičić, M.; Liang, X.; Mi, L.; Tričković, J. F.; Šobot, A. V.; Stanković, M. N.; Nakarada, Đ. Controlled killing of human cervical cancer cells by combined action of blue light and C-doped TiO2 nanoparticles. *Photochem. Photobiol. Sci.* **2021**, *20*, 1087.
(19) Kargar, F.; Bemani, A.; Sayadi, M. H.; Ahmadpour, N. Synthesis of modified beta bismuth oxide by titanium oxide and highly efficient solar photocatalytic properties on Hydroxychloroquine degradation and pathways. *J. Photochem. Photobiol., A* **2021**, *419*, 113453.
(20) Fang, F.; Liu, Y.; Sun, X.; Fu, C.; Prakash Bhoi, Y. P.; Xiong, W.; Huang, W. TiO2 Facet-dependent reconstruction and photocatalysis of CuOx/TiO2 photocatalysts in CO2 photoreduction. *Appl. Surf. Sci.* **2021**, *564*, 150407.
(21) Ola, O.; Maroto-Valer, M. M. Review of material design and reactor engineering on TiO2 photocatalysis for CO2 reduction. *J. Photochem. Photobiol., C* **2015**, *24*, 16−42.
(22) Tahir, M.; Tahir, B.; Saidina Amin, N. A. S.; Alias, H. Selective photocatalytic reduction of CO2 by H2O/H2 to CH4 and CH3OH over Cu-promoted In2O3/TiO2 nanocatalyst. *Appl. Surf. Sci.* **2016**, *389*, 46−55.
(23) He, Y.; Wang, Y.; Zhang, L.; Teng, B.; Fan, M. High-efficiency conversion of CO2 to fuel over ZnO/g-C3N4 photocatalyst. *Appl. Catal., B* **2015**, *168−169*, 1−8.
(24) Adekoya, D. O.; Tahir, M.; Amin, N. A. S. g-C 3 N 4 /(Cu/TiO2) nanocomposite for enhanced photoreduction of CO 2 to CH 3 OH and HCOOH under UV/visible light. *J. CO2 Util.* **2017**, *18*, 261−274.
(25) Pellegrin, Y.; Odobel, F. Sacrificial electron donor reagents for solar fuel production. *C. R. Chim.* **2017**, *20*, 283−295.
(26) Zhang, X.; Huang, Y.; Yang, J.; Gao, H.; Huang, Y.; Luo, X.; Liang, Z.; Tontiwachwuthikul, P. Amine-based CO2 capture aided by acid-basic bifunctional catalyst: Advancement of amine regeneration using metal modified MCM-41. *Chem. Eng. J.* **2020**, *383*, 123077.
(27) Yang, H.; Xu, Z.; Fan, M.; Gupta, R.; Slimane, R. B.; Bland, A. E.; Wright, I. Progress in carbon dioxide separation and capture: A review. *J. Environ. Sci.* **2008**, *20*, 14−27.
(28) Goeppert, A.; Czaun, M.; May, R. B.; Prakash, G. S.; Olah, G. A.; Narayanan, S. Carbon dioxide capture from the air using a polyamine based regenerable solid adsorbent. *JACS* **2011**, *133*, 20164−20167.
(29) Tseng, C.-L.; Chen, Y.-K.; Wang, S.-H.; Peng, Z.-W.; Lin, J.-L. 2-Ethanolamine on TiO2 investigated by in situ infrared spectroscopy. Adsorption, photochemistry, and its interaction with CO2. *J. Phys. Chem. C* **2010**, *114*, 11835−11843.
(30) Hospital-Benito, D.; Lemus, J.; Moya, C.; Santiago, R.; Ferro, V. R.; Palomar, J. Techno-economic feasibility of ionic liquids-based CO2 chemical capture processes. *Chem. Eng. J.* **2021**, *407*, 127196.
(31) An, X.; Yu, C. Y. Graphene-based photocatalytic composites. *RSC Adv.* **2011**, *1*, 1426−1434.
(32) Xiang, Q.; Yu, J.; Jaroniec, M. Graphene-based semiconductor photocatalysts. *Chem. Soc. Rev.* **2012**, *41*, 782−796.
(33) Padmanabhan, N. T.; Thomas, N.; Louis, J.; Mathew, D. T.; Ganguly, P.; John, H.; Pillai, S. C. Graphene coupled TiO2 photocatalysts for environmental applications: A review. *Chemosphere* **2021**, *271*, 129506.
(34) Zhang, W.; Li, X.; Liu, S.; Qiu, J.; An, J.; Yao, J.; Zuo, S.; Zhang, B.; Xia, H.; Li, C. Photo-catalytic oxidation of 5-hydroxymethylfurfural over interfacial-enhanced Ag/TiO2 under visible light irradiation. *ChemSusChem* **2022**, *15*, No. e202102158.
(35) Zelekew, O. A.; Kuo, D.-H.; Yassin, J. M.; Ahmed, K. E.; Abdullah, H. Synthesis of efficient silica supported TiO2/Ag2O

heterostructured catalyst with enhanced photocatalytic performance. *Appl. Surf. Sci.* **2017**, *410*, 454−463.
(36) Zhou, W.; Liu, H.; Wang, J.; Liu, D.; Du, G.; Cui, J. Ag2O/TiO2 nanobelts heterostructure with enhanced ultraviolet and visible photocatalytic activity. *ACS Appl. Mater. Interfaces* **2010**, *2*, 2385−2392.
(37) Wang, L.; Zhu, B.; Cheng, B.; Zhang, J.; Zhang, L.; Yu, J. In-situ preparation of TiO2/N-doped graphene hollow sphere photocatalyst with enhanced photocatalytic CO2 reduction performance. *Chin. J. Catal.* **2021**, *42*, 1648−1658.
(38) Song, J.; Wang, X.; Chang, C.-T. Preparation and characterization of graphene oxide. *J. Nanomater.* **2014**, *2014*, 276143.
(39) Hummers, W. S., Jr; Offeman, R. E. Preparation of graphitic oxide. *JACS* **1958**, *80*, 1339.
(40) Ma, S.; Xue, J.; Zhou, Y.; Zhang, Z. Photochemical synthesis of ZnO/Ag2O heterostructures with enhanced ultraviolet and visible photocatalytic activity. *J. Mater. Chem. A* **2014**, *2*, 7272−7280.
(41) Alborzi, S.; Feyzi, F. Effect of heat stable salt bis-(2-hydroxyethyl) methylammonium formate on CO2 absorption in aqueous methyldiethanolamine solution. *J. Mol. Liq.* **2019**, *281*, 376−384.
(42) Khosravi, B.; Feyzi, F.; Dehghani, M. R.; Kaviani, S. Experimental measurement and thermodynamic modeling of CO2 solubility in aqueous solutions of morpholine. *J. Mol. Liq.* **2016**, *214*, 411−417.
(43) Park, M. K.; Sandall, O. C. Solubility of carbon dioxide and nitrous oxide in 50 mass methyldiethanolamine. *J. Chem. Eng. Data* **2001**, *46*, 166−168.
(44) Peng, D.-Y.; Robinson, D. B. A new two-constant equation of state. *Ind. Eng. Chem. Fundam.* **1976**, *15*, 59−64.
(45) Herrmann, J.-M. Heterogeneous photocatalysis: fundamentals and applications to the removal of various types of aqueous pollutants. *Catal. Today* **1999**, *53*, 115−129.
(46) Wang, Z.-Y.; Chou, H.-C.; Wu, J. C.; Tsai, D. P.; Mul, G. CO2 photoreduction using NiO/InTaO4 in optical-fiber reactor for renewable energy. *Appl. Catal., A* **2010**, *380*, 172−177.
(47) Yamashita, H.; Ikeue, K.; Anpo, M.Photocatalytic reduction of CO_2 with H_2O on various titanium oxide catalysts. ACS Symposium Series; ACS Publications, 2002 809, Chapter 22, pp 330−343. DOI: 10.1021/bk-2002-0809.ch022.
(48) Ola, O.; Maroto-Valer, M. M. Transition metal oxide based TiO2 nanoparticles for visible light induced CO2 photoreduction. *Appl. Catal., A* **2015**, *502*, 114−121.
(49) Yu, B.; Zhou, Y.; Li, P.; Tu, W.; Li, P.; Tang, L.; Ye, J.; Zou, Z. Photocatalytic reduction of CO2over Ag/TiO2nanocomposites prepared with a simple and rapid silver mirror method. *Nanoscale* **2016**, *8*, 11870−11874.
(50) Michalkiewicz, B.; Majewska, J.; Kądziołka, G.; Bubacz, K.; Mozia, S.; Morawski, A. W. Reduction of CO2 by adsorption and reaction on surface of TiO2-nitrogen modified photocatalyst. *J. CO2 Util.* **2014**, *5*, 47−52.
(51) Akple, M. S.; Low, J.; Qin, Z.; Wageh, S.; Al-Ghamdi, A. A.; Yu, J.; Liu, S. Nitrogen-doped TiO2 microsheets with enhanced visible light photocatalytic activity for CO2 reduction. *Chin. J. Catal.* **2015**, *36*, 2127−2134.
(52) Truong, Q. D.; Liu, J.-Y.; Chung, C.-C.; Ling, Y.-C. Photocatalytic reduction of CO2 on FeTiO3/TiO2 photocatalyst. *Catal. Commun.* **2012**, *19*, 85−89.
(53) Wu, J. C. S. Photocatalytic reduction of greenhouse gas CO2 to fuel. *Catal. Surv. Asia* **2009**, *13*, 30−40.
(54) Jacob-Lopes, E.; Revah, S.; Hernández, S.; Shirai, K.; Franco, T. T. Development of operational strategies to remove carbon dioxide in photobioreactors. *Chem. Eng. J.* **2009**, *153*, 120−126.
(55) Huang, Q.; Yu, J.; Cao, S.; Cui, C.; Cheng, B. Efficient photocatalytic reduction of CO2 by amine-functionalized g-C3N4. *Appl. Surf. Sci.* **2015**, *358*, 350−355.
(56) Marszewski, M.; Cao, S.; Yu, J.; Jaroniec, M. Semiconductor-based photocatalytic CO2 conversion. *Mater. Horiz.* **2015**, *2*, 261−278.
(57) Karamian, E.; Sharifnia, S. On the general mechanism of photocatalytic reduction of CO2. *J. CO2 Util.* **2016**, *16*, 194−203.
(58) Ahmadpour, N.; Sayadi, M. H.; Sobhani, S.; Hajiani, M. Photocatalytic degradation of model pharmaceutical pollutant by novel magnetic TiO2@ZnFe2O4/Pd nanocomposite with enhanced photocatalytic activity and stability under solar light irradiation. *J. Environ. Manage.* **2020**, *271*, 110964.
(59) Otgonbayar, Z.; Oh, W.-C. Photo-electrochemical reduction of CO2 to Methanol on Quaternary chalcogenide loaded Graphene-TiO2 ternary nanocomposite fabricated via Pechini method. *J. Inorg. Organomet. Polym. Mater.* **2022**, *32*, 2910.

https://doi.org/10.1021/acsomega.2c06753
ACS Omega 2023, 8, 3981−3991